Pressure-induced electron topological transitions in Ba-doped Si clathrate

J. S. Tse,[1,*] L. Yang,[2] S. J. Zhang,[3] C. Q. Jin,[3] Ch. J. Sahle,[4] C. Sternemann,[4] A. Nyrow,[4] V. Giordano,[5] J. Z. Jiang,[6]
S. Yamanaka,[7] S. Desgreniers,[8] and C. A. Tulk[2]

[1]*Department of Physics and Engineering Physics, University of Saskatchewan, Saskatoon, Canada S7N 5E2*
[2]*Oak Ridge National Laboratory, Oak Ridge, Tennessee, USA*
[3]*Institute of Physics, Chinese Academy of Sciences, PO Box 603, Beijing, 100190, People's Republic of China*
[4]*Technische Universität Dortmund, Fakultät Physik/DELTA, D-44221 Dortmund, Germany*
[5]*European Synchrotron Radiation Facility, BP 220, F-38043 Grenoble Cedex 9, France*
[6]*International Center for New-Structured Materials (ICNSM), Zhejiang University and Laboratory of New-Structured Materials,
Department of Materials Science and Engineering, Zhejiang University, Hangzhou, People's Republic of China*
[7]*Department of Applied Chemistry, Graduate School of Engineering, Hiroshima University, Higashi-Hiroshima 739-8527, Japan*
[8]*Laboratoire de physique des solides denses, Department of Physics, University of Ottawa, Ottawa, Ontario K1N 6N5, Canada*

Ba_8Si_{46} is the archetype of the Si clathrates family. X-ray diffractions have revealed an unusual homothetic isostructural transition at $\sim$14–16 GPa. Raman experiments, however, suggested even more transitions at lower pressure. We present evidence showing that successive electronic topological transitions are responsible for the transformations. It is shown that the electronic structure of Ba_8Si_{46} is easily perturbed by the environment. Reverse Monte Carlo calculations and *in-situ* resistivity measurements revealed continual changes in the structure and electrical properties upon compression. This finding is corroborated by results of x-ray Raman scattering study in the vicinity of the Ba $N_{4,5}$ and Si $L_{2,3}$ absorption edges.

I. INTRODUCTION

Si clathrates are formed from a 3D sp^3 Si framework with voids where metal atoms can be encaged. Depending on the encaged dopants, the clathrates exhibit a number of unusual thermal and electrical properties.[1–11] The polymorph with Na as guest was first synthesized in the early 1960s.[12] It was found that the electrical conductivity changed from semiconducting to metallic behavior depending on the amount of the doped Na. The change from an insulator to metal has been suggested to be akin to a Mott transition with increased Na concentration.[13] In spite of initial interests, the study of this class of compounds has remained dormant until the discovery of superconductivity in $(Na,Ba)_8Si_{46}$ and the finding of very low thermal conductivity in Na_8Si_{46},[4] which suggested this class of clathrate compounds can be potentially high-efficiency thermoelectric materials. The search for mechanisms responsible for the novel superconducting and anomalous thermal conductivity has been the subject of many recent studies.[14,15] Despite these efforts, the role of low-frequency localized Ba vibrations (rattling) and the collective Si framework vibrations to electron-phonon coupling is still under debate.[5,6,16] Isotropic compression is a sensitive technique to probe these interactions. High-pressure powder diffraction experiments identified an unusual reversible *homothetic* isostructural *volume collapse* at 14–16 GPa[7,8] and eventually amorphized at 49 GPa.[17] This observation is confirmed by a subsequent Raman study.[9] In the latter experiment, changes in spectral features further suggest two new phase transitions at $\sim$7 GPa and tentatively at $\sim$3 GPa. Strikingly, intensities of the Raman bands[9] assigned to localized vibrations of Ba were enhanced at 3–5 GPa but disappeared at pressures above 6.8 GPa until 15 GPa when they reappeared. The Raman results so far have defied a reasonable explanation. Using a variety of techniques from structural studies with reverse Monte Carlo method (RMC), probing the

unoccupied states with x-ray Raman scattering (XRS) spectroscopy, and the measurement of the transport property, it is shown that the electronic structure of Ba_8Si_{46} is very sensitive to changes in the Ba-Si and Si-Si interactions. The results presented here provide a consistent explanation of all available experimental observations, including the high-pressure Raman and x-ray Raman spectra, homothetic volume collapse of the unit cell, and disappearance of superconductivity.

II. EXPERIMENTAL DETAILS

The powder diffraction patterns used previously for Rietveld refinements[8,18] were used in the RMC modeling. Experimental details have been reported in Refs. 8 and 18 and will not be repeated here. In essence, *in-situ* high-pressure diffraction measurements on powder Ba_8Si_{46} clathrate samples in diamond anvil cells (DACs) using helium as the pressure transmission medium were performed at beamline BL10XU of SPring8, Japan, with an x-ray wavelength of 0.4969 Å. For the XRS measurement, no pressure medium was used. High-pressure Ba $N_{4,5}$ XRS spectra were measured with the sample in a panoramic DAC[19] at beamline ID16[20] of the European Synchrotron Radiation Facility scanning the energy of the incident x-ray beam at a fixed analyzer energy of 9.69 keV to measure energy losses between 80 and 110 eV with an overall energy resolution of 1.3 eV at an averaged momentum transfer of $q = 9.3 \pm 0.4 \, \text{Å}^{-1}$. Variable temperature and pressure resistances of the sample were measured with the four-probe technique using 18 μm gold wires as electrodes. *In-situ* measurements were made in a DAC using the four-probe method using MgO as the pressure transmitting medium. Independent measurements on two different samples but limited to lower pressure range using *h*-BN as the pressure transmitting medium gave similar trends. The pressure was

measured at room temperature before and after each cooling cycle. In all cases, the fluorescence from a ruby sphere embedded in the sample was used as the pressure calibrant.[21]

Electronic calculations were performed using the pseudopotential plane wave code Vienna *ab-initio* structure package[22] employing projected augmented potentials[23] for the Ba and Si atoms and the Perdew–Wang (PW91) density functional.[24] The semicore $5p$ orbitals of Ba are included in the valence region. A plane wave energy cutoff of 226 eV and a Monkorst–Pack $16 \times 16 \times 16$ k mesh[25] was used for wave function expansion and the Brillouin zone integration, respectively. For the Fermi surfaces, calculations were performed on 5,000 k points evenly distributed in a uniform grid.

III. REVERSE MONTE CARLO MODELING

It was revealed in an earlier study[8] the Ba atoms in the clathrate structure are statically disordered. Furthermore, the framework Si atoms become positionally disordered after the homothetic isostructural transition. Rietveld refinement on a single unit is not sufficient to capture fine details in local distortions. Reverse Monte Carlo (RMC) using RMCPOW[26] is able to model static and dynamic disorder in crystalline materials using powder diffraction data by matching calculated structure factors computed from the atomic positions of a structural model refined through an iterative process with the measured diffraction pattern. The diffraction data, which were used for previous Rietveld refinement,[8] have been masked for diamond peaks, calibrated, and corrected for detector coefficients. The background functions are very smooth, indicating weak diffuse scattering. In RMCPOW,[26] a fourth-order polynomial function is used to fit the background, which is adequate for the purpose. The essential feature of RMCPOW is that the structure factor calculated directly from a model supercell is matched against the measured intensity. In this procedure, there is no truncation error, and the requirement of data at large momentum transfer (Q range) is not essential. This method is most suitable for systems where Bragg scattering dominates and diffuse scattering is weak. In the present work, we employed the same procedure on the analysis of all datasets obtained from ambient to 30.5 GPa,[8] i.e. the starting atom positions, lattice parameters, and peak profile parameters were obtained from corresponding Rietveld analysis. All relevant parameters, such as the constraints on maximum displacement and coordination, are the same for all datasets. RMCPOW calculations were performed on a model systems consist of 27 648 atoms ($8 \times 8 \times 8$ unit cells). Three to five million MC moves were attempted with an acceptance ratio 0.55. The statistic is sufficiently accurate to sample the potential disordering of the atomic positions. The agreement factor, R_{wp}, generally reduced from $\sim$0.09 in the Rietveld refinement to below 0.03 in RMCPOW. The improvement indicates that the disorder is properly accounted by RMC modeling. It should be noted that RMC is not guaranteed to produce a unique structural solution. Since a uniform strategy and all the refined parameters are reasonable, we are confident from the comparison of results obtained at different pressures informative structural information can be obtained.

Since Ba atom has the largest scattering factor, information extracted for the Ba-Ba and Ba-Si distances should also

be most reliable (Fig. 1). Below 10 Å, the Ba-Ba distance distributions can be separated into two regions. As Ba occupy two different cages, the three peaks at ∼5.0, 5.7, and 6.3 Å correspond, respectively, to separations between Ba in neighboring large cages Ba(L), Ba in the small and neighboring large cages [Ba(S)-Ba(L)], and the second nearest neighbors between Ba(L). The second set of peaks can be assigned to longer Ba(S)-Ba(S) (9.0 Å), Ba(S)-Ba(L) (9.3 Å), and Ba(L)-Ba(L) (9.7 Å) correlations. To identify the possible phase transitions with increasing pressure, it is important to monitor consecutive changes to identify a critical pressure at which a measured quality changes abruptly. Initially, the width of the Ba-Ba pdf is about 0.25 Å. At low pressure, the immediate and second nearest Ba(L)-Ba(L) peak widths gradually become sharper, and at 6.2 GPa, the peak width decreases to 0.09 Å. In contrast, the width of the Ba(S)-Ba(L) correlation only changes slightly. A peculiar observation is made near 3.4 GPa, in which the Ba(L)-Ba(L) pdf peaks widened momentarily then become very sharp and almost independent of the pressure between 3.8–7.8 GPa. This result indicates the Ba-Si interactions are isotropic in the more spherical Si_{24} cages. Above 7.8 GPa, the Ba-Ba separations are shortened due to the compression, as expected, and widths of the distribution functions start to broaden again. From 18.6 to 30.5 GPa, the peak widths of the pdfs become narrower as the pressure increases.

Changes in the features of the Ba-Si pdf with pressure correlate well with the trend observed in the Ba-Ba pdfs. The Ba-Si pdf below 4 Å can be assigned to two groups. The shorter distance peak is assigned to Ba(S)-Si and the longer one to Ba(L)-Si. Below 7.8 GPa, the Ba(S)-Si correlations become better defined with increasing pressure. Near 6.2 GPa, as in the case of Ba-Ba correlations, features in the Ba-Si pdfs become very distinctive. In fact, the three resolved peaks can all be attributed to Ba(L)-Si correlations. A similar widening of all the peaks at 3.4 GPa is also observed. Once again, the features become broader from 7.8 to 12.4 GPa. Above 18.6 GPa, the first nearest neighbor Ba(S)-Si correlation peak becomes more distinct with increasing pressure. The first and second peaks on the Si-Si pdfs correspond to the nearest and next nearest neighbor Si-Si correlations. The most noticeable feature is that the peak widths start to increase at ∼15 GPa and become very broad at 18.6 GPa, which is like a temporary relaxation of the framework. The distinctive pdf pattern, however, was recovered with the two peaks continuing to widen at pressures above 18.6 GPa.

Several conclusions can now be drawn. Three structural transformations at 3.4, 7.8, and 18.6 GPa can be inferred from the RMC results. Below 3.4 GPa, Ba in the large cages are disordered and not statically situated at the ideal crystallographic sites. At 3.4 GPa, there is a temporary relaxation of the Ba positions, after which Ba in the large cage are frozen. The RMC results are in agreement with the trend in the Ba isotropic thermal parameter (B_{iso}) determined from Rietveld refinement.[8] In the experiment, B_{iso} of Si and Ba were found to decrease in this pressure region reflecting that the Ba are more ordered. At 7.8 GPa, the Ba's B_{iso} in the large cages increases, and so they become more disordered. At 18.6 GPa, there is a relaxation of the Si framework, causing the isosymmetric structural collapse. After the transition, the Ba_8Si_{46} structure
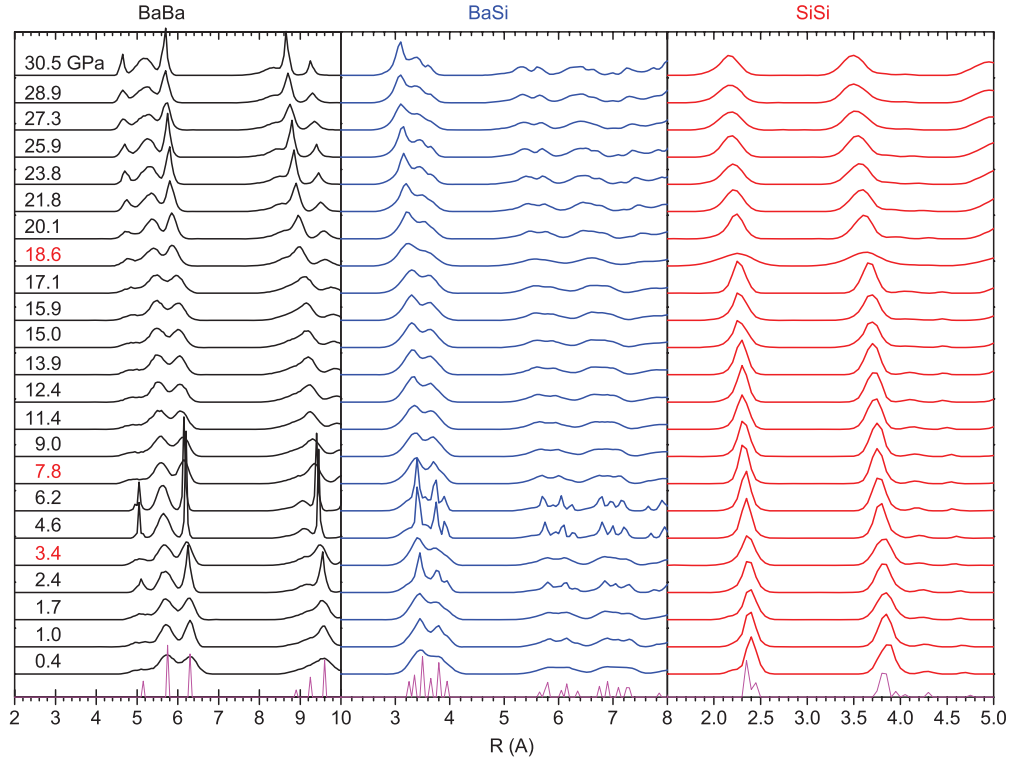
FIG. 1. (Color online) Pressure dependence of Ba-Ba, Ba-Si, and Si-Si pdf, partial distribution function (PDF) obtained from RMCPOW calculations on experimental diffraction data taken from Ref. 8. Ba and Si atoms were allowed to move with a maximum stepsize of 0.1 and 0.05 Å, respectively. Coordination confinements, i.e. tetragonal coordination, were applied for the framework Si. The red (dark gray) stick diagrams correspond to the relevant atom separations in the ideal crystal at zero pressure. Pressure at the three plausible structural transformations is highlighted in red (dark gray).

can be described as a positional disordered Si framework with Ba still located in their respective crystallographic sites, and as the pressure increases, the Ba atoms become more ordered again. This suggests the two low-pressure transformations are related to changes in the electronic state of Ba atoms in the large cages, and the third transformation is associated with disordering in the Si framework.

The pressure-induced structural changes in Ba_8Si_{46} can now be used to explain the Raman spectra. In the Raman study,[9] the intensity and the profile of localized vibrational bands of the encaged Ba were found to change continuously from 0 to 5.4 GPa with the spectral features becoming sharper as the pressure is increased. This observation corresponds to increased ordering of Ba in the large cages as reflected in the narrowing of the width of the inter-cage Ba(L)-Ba(L) correlations. At pressures higher than 6.2 GPa, the Ba become more localize and displace slightly from the ideal crystallographic positions, and the site symmetry becomes higher. Factor group analysis has shown that the zone center modes for Ba in the small cages transformed as $T_{1u} + T_{2u}$, and so they are Raman inactive.[27] Several zone center modes due to disordered Ba in the large cages should also vanish. This explains the loss of intensities in the Raman band. The onset of the structural transition is at 12.4 GPa and completed at 18.6 GPa. It is already known that the transition is the result of the rehybridization of the framework Si atoms,[18] and the RMC calculations show the Si atoms are likely positional disordered.

Therefore, the site symmetry at the Ba is lost again, and this led to the reemergence of the low-frequency Ba Raman vibrations. Moreover, the very broad and featureless Si vibrations also support the view that the Si framework atoms are positionally disordered.

IV. X-RAY RAMAN SPECTRA

X-ray absorption spectra are sensitive to changes in atomic and electronic structure. Previous Ba L_3 absorption spectra have been measured with the conventional transmission method, which are limited to low momentum transfer (i.e. $q = 0$) and only probed the dipolar $p \rightarrow d$ excitations.[17] An energy shift of the Ba edge positions to smaller energies with increasing pressure was observed, and the white line intensity increases for pressures above 10 GPa, which was attributed to a distorted Ba environment. Here, XRS,[28] an energy loss spectroscopy, is employed to measure the Ba $N_{4,5}$ and Si $L_{2,3}$ edges spectra. The Ba $N_{4,5}$ edge was chosen since, apart from taking advantage of the sensitivity of the $d \rightarrow f$ giant resonance on the environment,[29] nondipolar transitions observed at high-momentum transfer can provide more information on the density of unoccupied states. Details of the analysis can be found elsewhere.[30] X-ray Raman scattering spectra were measured between 1.5 and 19.4 GPa [Fig. 2(a)]. For energy losses between 92 and 99 eV, the strong Ba multiplet lines in the vicinity of the Ba $N_{4,5}$ edge
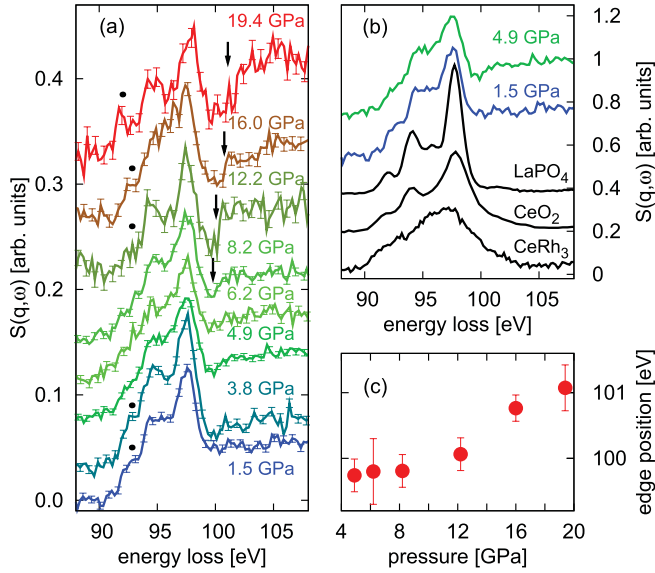
FIG. 2. (Color online) (a) X-ray Raman spectra, $S(q, \omega)$, of the Ba $N_{4,5}$ and Si $L_{2,3}$ edges of Ba_8Si_{46} as a function of pressure. (b) Comparison of spectra at 1.5 and 4.9 GPa with results for $LaPO_4$, CeO_2, and $CeRh_3$ of Gordon *et al.* (Ref. [31]). The spectra of CeO_2 and $CeRh_3$ were shifted by -14 eV, the spectrum of $LaPO_4$ by -7.4 eV on the energy loss scale. The position of the absorption edge is determined by a fit of the spectra in between 99 and 108 eV using a tanh function. (c) Onset of the Si $L_{2,3}$ absorption edge as a function of pressure.

can be observed, whereas for energy losses above 99 eV, the contribution of the Si $L_{2,3}$ edge dominates the XRS spectra. The shape of the Ba multiplet resembles that of other materials measured at high-momentum transfer in which interaction with $4f$ states plays an important role.[31] All features observed for Ba at the $N_{4,5}$ edge of the Si clathrate can also be observed for Ce and La. These are the multiplet features appearing in the nondipole limit and the giant resonance in the dipole limit. The three-peak structure observed in the Ba $N_{4,5}$ spectra is typical of the Ce^{4+} $4d^{10}f^0 \rightarrow 4d^9f^1$ multiplet nondipole transitions observed in CeO_2.[31] The spread of the peaks is about 8 eV and is smaller than in CeO_2 ($\sim$10 eV). This is consistent with the lower nuclear charge of Ba. The most important similarities of these systems are the free $4f$ states and excitation from $4d$ levels. This, and not the different valence configurations, leads us to the comparison made. This point is strengthened from a comparison between Ba_8Si_{46} and $BaSO_4$ XRS spectra[32] measured at low-momentum transfers (Fig. 3). Here, also clear evidence is found that the multiplet features are less pronounced in the Si clathrate. The peak profile of Ba_8Si_{46} multiplet is somewhat broadened between 4.9 and 6.2 GPa, as indicated by vanishing of both the first feature at 92.8 eV [dot in 2(a)] and the dip at 96.0 eV. The broadening can be interpreted as the result of stronger covalent interactions between Ba and Si. This is emphasized by comparison of the Ba_8Si_{46} XRS spectra measured at 1.5 and 4.9 GPa with results obtained for analogous $LaPO_4$, CeO_2, and $CeRh_3$.[31] With increasing hybridization, the spectra are significantly smeared out [see Fig. 2(b)]. The observed broadening is in line with diffraction results, showing that Ba atoms are situated in the crystallographic symmetry sites
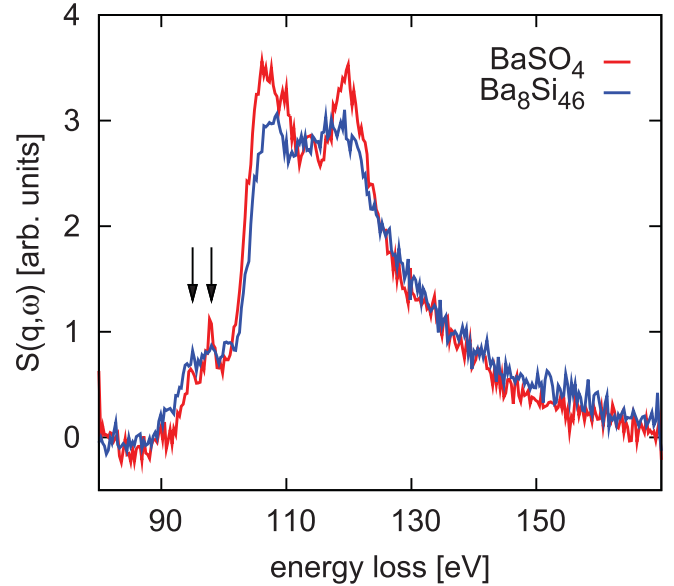

FIG. 3. (Color online) Comparison of the Ba $N_{4,5}$ x-ray Raman spectra of Ba_8Si_{46} and $BaSO_4$ (Ref. [32]) showing the multiplet features before the onset of the giant resonance.

in this pressure range. At 12.2 GPa, the multiplet structures sharpen again, and the energy loss position of the multiplet peaks change slightly at the highest pressure of 19.4 GPa. The sharper multiplet structure indicates changes in the Ba-Si interaction, which is again in line with the diffraction results, which suggest increasing disorder in the Si cages. The most prominent features in the Si $L_{2,3}$ absorption edge is the shift to higher energy losses, as shown by arrows in Fig. 2(a), accompanied by an increase in intensity for energy losses above 102 eV. Positions of the absorption edge are presented in Fig. 2(c). These observations suggest an increase in ionicity of the Si atoms by transfer of electrons from the Si site to the interstitial regions.[18,33] This finding is again consistent with the picture that Si atoms rehybridize[18,33] from sp^3 to spd. The participation of the Si $3d$ orbitals in chemical bonding allows a charge transfer from Si to the Ba atoms, slightly increasing the charge.

V. TRANSPORT PROPERTIES

The subtle changes in the short-range order revealed from RMC, Raman, and XRS experiments may manifest themselves in the electrical properties. To this end, the electrical resistance of Ba_8Si_{46} as a function of pressure was measured from 80 to 280 K. The results at 90 and 280 K are compared in Fig. 4(a). The resistances were found to decrease when the pressure increases. There is no significant difference in the resistance for the two temperatures at pressures lower than 10 GPa. At higher pressure, the resistance at 280 K is higher than 80 K. This behavior indicates that Ba_8Si_{46} is a poor metal at low pressure and becomes a true metal at high pressure. Discontinuities in the resistance are identified at 4, 7, and 16 GPa. These pressures correlate well with the structural changes revealed by RMC calculations and the observed spectral features in the Raman spectra. The temperature profile of the resistance changed at the transitions [Fig. 4(b)]. At low pressure ($0 <$
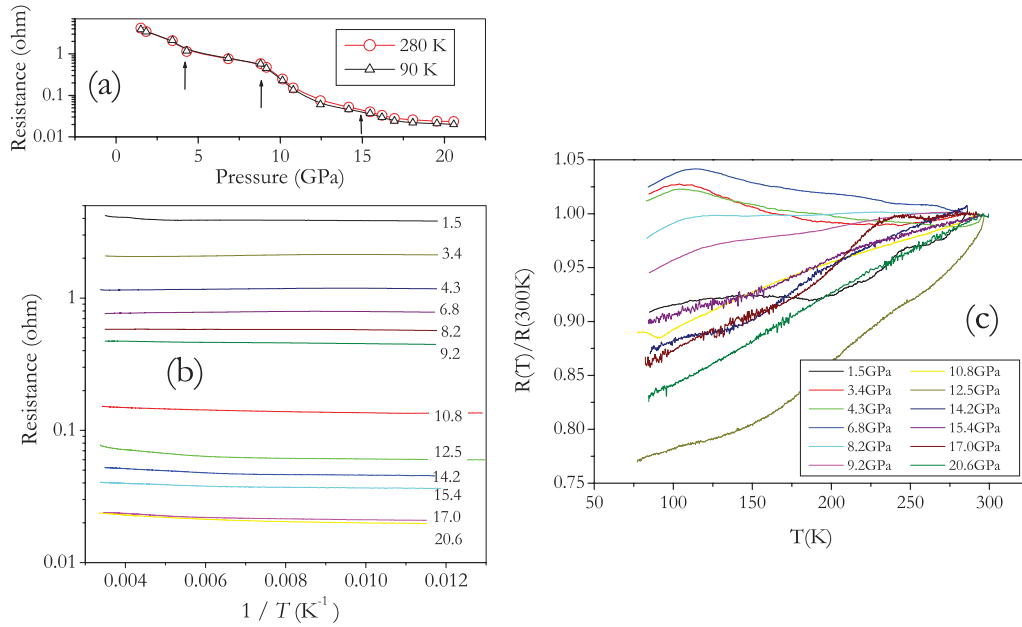
FIG. 4. (Color online) (a) Comparison of the electrical resistance of Ba_8Si_{46} measured at 80 and 280 K. The arrows indicated possible electronic transitions. (b) A comparison of the temperature dependence of the electrical resistance of Ba_8Si_{46} relative to 300 K at selected pressures. (c) Plot of the ratio of the resistance (R) at temperature T relative to that at 300 K.

5 GPa), the resistance increases rapidly at high temperature. Between 4–8 GPa, the resistance is largely constant. Above 8 GPa, the resistance increases steadily with temperature. Finer details in the variation of the resistance (R) with temperature are exemplified in the plot of the ratio $R(T)/R(300)$ [Fig. 4(c)].

A discontinuity in the electrical resistance signifies a change in the conduction band electron topology. This is supported by the calculated Fermi surfaces (FSs) (Fig. 5). Below 5 GPa, four electronic bands cross the Fermi level. The FSs of these bands are shown in Fig. 5. Except for the highest energy (fourth) band, the FSs are very complex and extended over the entire Brillouin zone. The spherical FS of the fourth band indicates free electron character of this higher-energy band.

FIG. 5. (Color online) Calculated Fermi surface (FS) of Ba_8Si_{46} at 5, 9, and 16 GPa.

Interestingly, the second band shows several parallel sheets which are favorable to the nesting of the FS, an important contributing factor of superconductivity.[34] At 9 GPa, only three electronic bands cross the Fermi level. The topology of the former second band has changed substantially. The FS becomes more open, and there is a loss of parallel sheets. The latter may be related to the diminished superconductivity under applied pressure.[11] The second band now forms necks and connects to the next Brillouin zones. The spherical FS has grown larger. At 16 GPa, there are significant changes in all the FSs. The third electronic band is no longer spherical, but distorted, and developed depressions in the middle of the surfaces. In addition, the necks connecting neighboring Brillouin zones have also grown much larger.
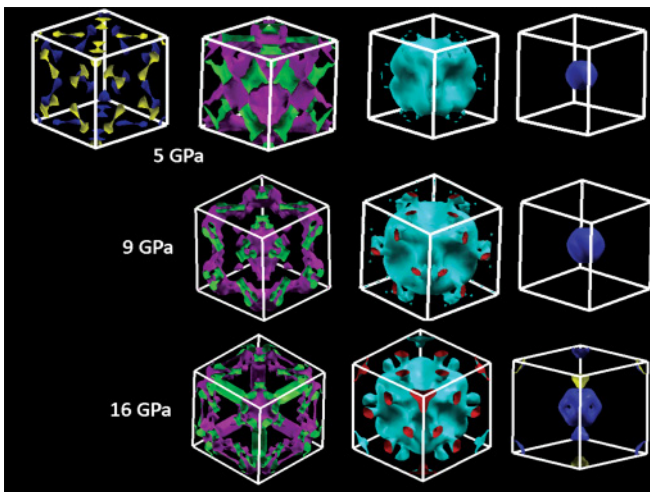
VI. CONCLUSIONS

In summary, experimental and theoretical results presented here show unambiguously three electronic transitions at 4, 7, and 16 GPa. These phenomena can be classified as electron topological transitions,[10] where the electronic structure is modified due to changes in the interactions between Ba and Si at low pressures and, as shown earlier,[17] rehybridization of Si at high pressure without affecting the crystal symmetry. This conclusion agrees with the observation of a 0.4-eV shift in the Ba L_{III} XAS[16] and the collapse of the cage structure of related $Ba_{24}Si_{100}$, which has also been attributed to the disordering of the Si framework.[35]

*Corresponding author: jst634@mail.usask.ca

[1] R. G. Ross, P. Andersson, and G. Backström, Nature **290**, 322 (1981).

[2] J. L. Cohn, G. S. Nolas, V. Fessatidis, T. H. Metcalf, and G. A. Slack, Phys. Rev. Lett. **82**, 779 (1999).

[3] H. Kawaji, H. O. Horie, S. Yamanaka, and M. Ishikawa, Phys. Rev. Lett. **74**, 1427 (1995).

[4] J. S. Tse, K. Uehara, R. Rousseau, A. Ker, C. I. Ratcliffe, M. A. White, and G. MacKay, Phys. Rev. Lett. **85**, 114 (2000).

[5] K. Tanigaki, T. Shimizu, K. M. Itoh, J. Teraoka, Y. Moritomo, and S. Yamanaks, Nat. Mater. **2**, 653 (2003).

[6] R. Lortz, R. Viennois, A. Petrovic, Y. Wang, P. Toulemonde, C. Meingast, M. M. Koza, H. Mutka, A. Bossak, and A. San Miguel, Phys. Rev. B **77**, 224507 (2008).

[7] A. San-Miguel, P. Mélinon, D. Connétable, X. Blase, F. Tournus, E. Reny, S. Yamanaka, and J. P. Itié, Phys. Rev. B **65**, 054109 (2002).

[8] L. Yang, Y. M. Ma, T. Iitaka, J. S. Tse, K. Stahl, Y. Ohishi, Y. Wang, R. W. Zhang, J. F. Liu, H. K. Mao, and J. Z. Jiang, Phys. Rev. B **74**, 245209 (2006).

[9] T. Kume, H. Fukuoka, T. Koda, S. Sasaki, H. Shimizu, and S. Yamanaka, Phys. Rev. Lett. **90**, 155503 (2003).

[10] M. Lifshitz, Sov. Phys. JETP **11**, 1130 (1960).

[11] D. Connétable, V. Timoshevskii, B. Masenelli, J. Beille, J. Marcus, B. Barbara, A. M. Saitta, G. M. Rignanese, P. Mélinon, S. Yamanaka, and X. Blasé, Phys. Rev. Lett. **91**, 247001 (2003).

[12] J. S. Kasper, P. Hagenmuller, M. Pouchard, and C. Cros, Science **150**, 1713 (1965).

[13] N. F. Mott, Rev. Mod. Phys. **50**, 203 (1978).

[14] M. M. Koza, M. R. Johnson, R. Viennois, H. Mutka, L. Girard, and D. Ravot, Nat. Mater. **7**, 805 (2008).

[15] M. Christensen, A. B. Abrahamsen, N. B. Christensen, F. Juranyi, N. H. Andersen, K. Lefmann, J. Andreasson, C. R. H. Bahl, and Bo B. Iversen, Nat. Mater. **7**, 811 (2008).

[16] J. S. Tse, T. Iitaka, and K. Parlinski, Europhys. Lett. **75**, 153 (2006).

[17] A. San Miguel, A. Merlen, P. Toulemonde, T. Kume, S. Le Floch, A. Aouizerat, S. Pascarelli, G. Aquilanti, O. Mathon, T. Le Bihan, J. P. Itie, and S. Yamanaka, Europhys. Lett. **69**, 556 (2005).

[18] J. S. Tse, R. Flacau, S. Desgreniers, T. Iitaka, and J. Z. Jiang, Phys. Rev. B **76**, 174109 (2007).

[19] R. Lübbers, H. F. Grünsteudel, A. I. Chumakov, and G. Wortmann, Science **287**, 1250 (2000); H. Giefers, R. Lübbers, K. Rupprecht, G. Wortmann, D. Alfie, and A.I. Chukov, High Press. Res. **22**, 502 (2002).

[20] R. Verbeni, T. Pylkkänen, S. Huotari, L. Simonelli, G. Vanko, K. Martel, C. Henriquet, and G. Monaco, J. Synchrotron Rad. **16**, 469 (2009).

[21] H. K. Mao, P. M. Bell, J. W. Shaner, and D. J. Steinberg, J. Appl. Phys. **49**, 3276 (1978).

[22] G. Kresse and J. Furthmuller, Comput. Mater. Sci. **6**, 15 (1996); Phys. Rev. B **54**, 11169 (1996).

[23] G. Kresse and D. Joubert, Phys. Rev. B **59**, 1758 (1999).

[24] J. P. Perdew, in *Electronic Structure of Solids '91*, edited by P. Ziesche and H. Eschrig (Akademie Verlag, Berlin, 1991), p. 11.

[25] H. J. Monkhorst and J. D. Pack, Phys. Rev. B **13**, 5188 (1976).

[26] A. Mellergrad and R. L. McGreevy, Acta Cryst., A **55**, 783 (1999).

[27] J. S. Tse, C. I. Ratcliffe, B. M. Powell, V. F. Sears, and Y. P. Handa, J. Phys. Chem. A **101**, 4491 (1997).

[28] W. Schülke, *Electron Dynamics by Inelastic X-ray Scattering* (Oxford University Press, Oxford, 2007).

[29] H. Sternemann, C. Sternemann, J. S. Tse, S. Desgreniers, Y. Q. Cai, G. Vankó, N. Hiraoka, A. Schacht, J. A. Soininen, and M. Tolan, Phys. Rev. B **75**, 245102 (2007).

[30] H. Sternemmann, C. Sternemann, G. T. Seidler, T. J. Fuster, A. Sakko, and M. Tolan, J. Synchrotron Rad. **15**, 162 (2008).

[31] R. A. Gordon, G. T. Seidler, T. T. Fister, M. W. Haverkort, G. A. Sawatzky, A. Tanaka, and T. K. Sham, Europhys. Lett. **81**, 26004 (2008).

[32] C. Sternemann, H. Sternemann, S. Huotari, F. Lehmkuhler, M. Tolan, and J. S. Tse, J. Anal. At. Spectroscopy **23**, 807 (2008).

[33] J. S. Tse, Z. Krist. **220**, 521 (2005).

[34] D. Kasinathan, J. Kunes, A. Lazicki, H. Rosner, C. S. Yoo, R. T. Scalettar, and W. E. Pickett, Phys. Rev. Lett. **96**, 047004 (2006).

[35] P. Toulemonde, D. Machon, A. San Miguel, and M. Amboage, Phys. Rev. B **83**, 134110 (2011).